Early Detection of Oral Cancer through textural analysis of histopathological images of oral submucous fibrosis

Synopsis of the Thesis to be submitted in partial fulfillment

of the requirements for the degree of

Masters of Technology (Hons.)

In

Electrical Engineering

By

Anirudh Choudhary

05EE3008

Under the guidance of

Prof. Jayanta Pal

Department of Electrical Engineering
Indian Institute of Technology Kharagpur
INDIA-721302

May 2009 – April 2010

Department of Electrical Engineering,

Indian Institute of Technology,

Kharagpur-721 302

INDIA

CERTIFICATE

This is to certify that the work presented in this thesis entitled "**Early Detection of Oral Cancer through textural analysis of histopathological images of oral submucous fibrosis**" submitted by **Mr. Anirudh Choudhary (Roll No: 05EE3008)** in partial fulfillment of the requirements for the award of the degree of **Master of Technology (Hons)** is a bonafide record of work carried out by him under my supervision. To the best of my knowledge and belief, it has not been submitted to any other institute or university for the award of any degree or diploma.

Professor Jayanta Pal

Professor, Electrical Engineering

Department of Electrical Engineering

Indian Institute of Technology Kharagpur-721302

West Bengal, INDIA

5th May, 2010

ACKNOWLEDGEMENTS

First and foremost, I would like to thank my project guide Prof. Jayanta Pal who has been more of a friend and much more than just an advisor. I would like to thank him for the freedom and flexibility given to formulate the idea and develop the algorithms. Next, I would thank my B.Tech project guide Prof. A.K. Ray for introducing me to the field of Medical Image Processing and for his support and encouragement throughout the project. His ingenuous outlook on research problems taught me the basics of research.

I would also like to express my gratitude towards Mr. M. Muthuramakrishnan for providing me the image datasets & helping me with the derivation of mathematical formulae.Chapter 2 & Chapter 4 are a direct direct consequence of my work carried out along with him.I am thankful to some of my dual degree friends who have stood by me in time of need and also found out time to listen to my problems whenever I got stuck.

Finally, I would like to thank my parents, *Mr. Rameshwar Lal* and *Mrs. Jaya* and my school teachers who have always been a source of encouragement for all my endeavors. I cannot adequately express how much I owe this to them.

Abstract

Oral cancer is almost always preceded by certain oral pre-cancerous lesions and conditions among which oral sub mucous fibrosis (OSF) is the most common and potent pre-cancerous condition. Textural information plays a significant role in tissue characterization and diagnosis, in addition to morphology and intensity. The aim of this work is to improve the classification accuracy based on textural features for the development of a computer assisted screening of oral sub-mucous fibrosis (OSF). In totality, 61 textural features are extracted from epithelial region of the tissue sections using 2 wavelet families, Gabor-wavelet & local binary pattern. All 61 features extracted from the textural descriptors are statistically significant ($p<0.05$) in discriminating the OSF & normal cases. Based on classification accuracy, the best wavelet family i.e, db4 is selected for classifier design. SVM base classifier is trained & tested using 99 samples based on 61 textural features and its classification accuracy is computed for each of the combinations of wavelet family and rest of the extractors. Finally, it has been investigated that db4 wavelet coefficients leads to higher accuracy (90.09%) in combination with other features through k-fold cross validation. A new epithelial layer segmentation method based on combination of intensity & texture gradient based watershed has been proposed and is found to be superior to the Otsu thresholding method previously used. Robust cell segmentation based on marker based watersheds & GVF snake is employed & 12 cell features are extracted for cell classification into normal or OSF case. Implementation of presented algorithms is done in MATLAB. The results support the capability of multidimensional textural methods to capture the change in texture of epithelium with respect to the progression of cancer.

Contents

List of Figures

CHAPTER ONE

Introduction

In recent years there has been an increase in the cancers of the oral cavity and each year more than 0.3 million new cases [1] of oral cancer are reported. A high incidence of oral cancer [2] is mainly due to late diagnosis of potential precancerous lesions and conditions. Oral cancer develops from preexisting precancerous oral lesions. The common oral precancerous lesions are leukoplakia, erythroplakia, oral sub-mucous fibrosis etc. The precancerous status is judged on the basis of light microscopic histopathological features of oral epithelial dysplasia (OED) and/or cellular atypia which have different grades according to involvement of the epithelial region. Oral Submucous Fibrosis (OSF) is an insidious chronic progressive precancerous condition with a high degree of malignant potentiality. A large number of these cases transform into Oral Cancer. Moreover, dysplasia depicts associated epithelial hyperplasia or even rarely epithelial atrophy [3-5]. Interestingly epithelial hyperplasia may be noted in early stage of OSF while epithelial atrophy is consistent with advance stage [6]. This hyperplasic or atrophic status may also change the texture of the epithelium.

The most effective way to control oral cancer is to combine early diagnosis and timely and appropriate treatment. Because more than 90% of all oral cancers are squamous cell carcinomas, the vast majority of oral cancers will be diagnosed from lesions on the mucosal surfaces. Presently, in diagnosis of OSF and their grading with respect to progression and malignant potentiality, mainly qualitative histopathological techniques & biopsies are applied.

A means of inspecting histopathological characteristics at a molecular or cellular level is the motivation for the use of microscopic imaging. Although it is an invasive procedure, this modality has the advantage of providing high resolution images exposing the richness or denseness of the examined

underlying texture as compared to other non-invasive imaging modalities. It assists in giving a better interpretation to histopathological images, through studying the effect of disease on the cellular characteristics of the body tissue. This is done by staining the extracted tissue biopsies with dyes for visual contrast improvement, which will then facilitate the delineation of cell nuclei, giving a better tissue characterization. Despite this modality being invasive, which is unpleasant for patients, physicians usually require a biopsy for a definite answer if they are suspicious about a certain abnormality in an image acquired by a non-invasive imaging modality, and a closer view of the histopathological specimens can assist in verifying the tumour type.

Pathologists have been using microscopic images to study tissue biopsies for a long time, relying on their personal experience on giving decisions about the healthiness state of the examined biopsy. This includes distinguishing normal from abnormal (i.e. cancerous) tissue. Nevertheless, variability in the reported diagnosis may still occur due to the heterogeneous nature of the diseases; ambiguity caused by nuclei overlapping; noise arising from the staining process of the tissue samples; intra-observer variability and inter-observer variability. Therefore, over the past three decades, quantitative techniques have been developed for computer-aided diagnosis, which aims to avoid unnecessary biopsies and assist pathologists in the process of cancer diagnosis [10]. Since the Oral Submucous Fibrosis starts within the epithelial layer, hence the epithelial layer will be the first to undergo any changes in cell orientation, color as well as cell density & hence its analysis can be used for early diagnosis & detection of oral lesion. Texture is a representative of the morphological features of the epithelial layer & capturing the texture information of the epithelial layer is important for understanding the underlying patho-physiological changes from normal to OSF. A number of research studies have been done in analyzing histopathological images for cancer detection in various organs. Some attempts for texture quantification are based on wavelet transform [11-13] for early detection of lung cancer and neuroblastoma. In [14, 15], Gabor filter based texture analysis is performed on

mammography images and liver ultrasound images. Using more than one measure for classification is applied as well, such as using spatial and frequency texture features for classification by regression trees analysis [16]. Some used morphological characteristics for feature extraction [17] and others focused more on classifier improvement [18].

However, no specific quantitative histopathological evaluation procedure based on texture is available to assess and analyze the vital changes in the cell arrangement in oral mucosa. In view of this, a systematic approach combining multi-scale textural techniques & cellular features is devised in order to provide better understanding of textural changes over normal and OSF tissue sections. Chapter 2 outlines the texture feature extraction of the epithelium layer and classification of histopathological images into normal & OSF cases using SVM based classifier. The best wavelet family i.e., db4 is selected based on mean distance criteria and it is combined with other textural features for achieving the highest classification accuracy. Support Vector Machines based classifier is validated using *k*-fold cross-validation approach. Chapter 3 deals with improvement of the segmentation of epithelium layer using a texture gradient based watershed segmentation & color based region merging. The first part of the chapter focuses on Gabor filter based watershed segmentation while the second part describes a combined color & texture based multistage region merging. In Chapter 4, cell segmentation using seeded watershed followed by the application of GVF based snakes is presented & cell features are extracted and classified. Finally, conclusions are drawn in Chapter 5.

CHAPTER TWO

Textural Analysis of Epithelial Layer

Texture is an important property of surfaces which characterizes the nature of the surface. An important task in image processing and machine vision is the task of segmenting regions of different texture in an image. However, images of real objects often do not exhibit regions of uniform intensities. For example, the image of epithelium layer is not uniform but contains variations of densities of cells which form certain repeated patterns called visual texture. The patterns can be the result of physical surface properties such as roughness or oriented cells which often have a tactile quality, or they could be the result of reflectance differences such as the color on a surface.

67 and 32 images of surface epithelium from normal oral mucosa and OSF with dysplasia are optically grabbed by Zeiss Observer.Z1 Microscope (Carl Zeiss, Germany) using H&E stained histological sections under 10x objective (NA 0.25).At a resolution used of 1.33 μm and the pixel size of 0.63 μm, the grabbed digital images having dimension 1388×1040 have been stored in the computer. The first step in textural analysis is the segmentation of the epithelium layer. Since the epithelium layer has darker intensity than the surrounding tissues, a thresholding based method has been implemented.

2.1 Segmentation of the epithelial layer

The histopathological image of oral mucosa grabbed by Carl Zeiss microscope contains white and black pixels (random noise) & staining color variations. To smoothen out the variations and remove the noise, a 5x5 median filter is applied followed by histogram based adaptive contrast enhancement [19] thus normalizing the staining variations. Otsu based

thresholding is applied to roughly segment out the epithelial layer.Since the epithelial layer has redundant edge pixels due to the cells attached to it, post processing is required. Edge detection and morphological operations are performed to remove smaller regions and fill the holes within the epithelial layer. Redundant edges left over are removed using local edge linking. Most edge detectors yield information about the magnitude of the gradient & the direction of the edge in the locality of the point. This is useful in deciding which edge points to link together since edge points in a neighbourhood which have similar gradients directions are likely to lie on the same edge. Local edge linking methods usually start at some arbitrary edge point and consider points in a local neighbourhood for similarity of edge direction. If the points satisfy the similarity constraint then the points are added to the current edge set. If the points do not satisfy the constraint then we conclude we are at the end of the edge, and so the process stops. A new starting edge point is found which does not belong to any edge set found so far, and the process is repeated. The algorithm terminates when all edge points have been linked to one edge or at least have been considered for linking once.

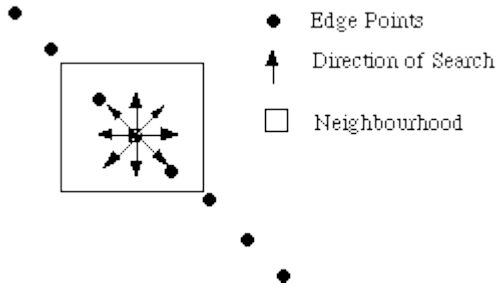

Fig. [3.1] Points considered in edge linking

Connected component labeling is performed to label the edges and the closed contour having the largest length is extracted. This contour defines the boundary of the epithelium layer and is superimposed upon the

original image to segment the epithelium layer as shown in Fig [3.2].

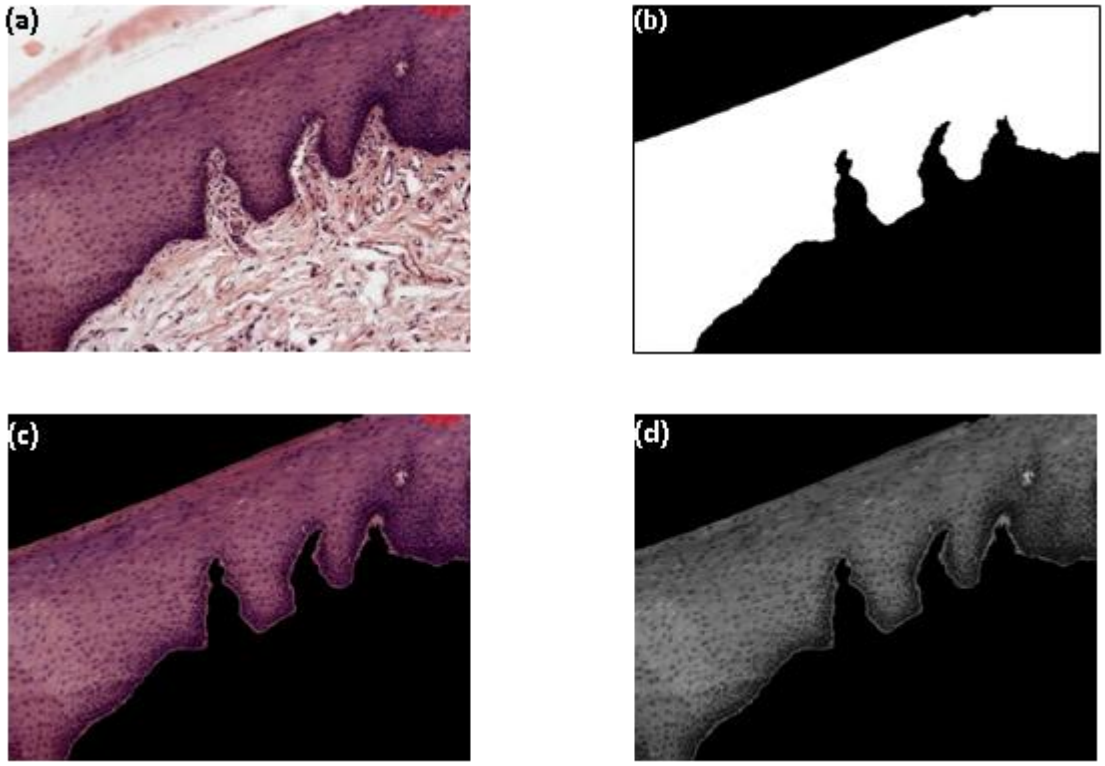

Fig [2.2]. Segmentation of epithelial layer (a) Normal oral mucosa image; (b) Epithelial layer extraction from (a); (c) AND operation between (a) and (b); (d) Gray scale image of (c)

2.2 Multi-scale Textural Features

The epithelium is composed by 4 layers and each layer's cells have unique morphological arrangement in a well-organized manner leading to textural variation. This variation gives the textural changes occurred during progression of cancer from normal which can be quantified by following multi-scale textural features based methods:

2.2.1 Wavelet decomposition based techniques

Wavelets are a class of functions used to localize a given function in both space and scaling. A family of wavelets can be constructed from a function known as a mother wavelet, which is confined in a finite interval. Daughter wavelets are then formed by translation(b) and contraction(a).Wavelets

are superior over traditional Fourier methods in analyzing physical situations where the image contains discontinuities and sharp spikes.

An individual wavelet is defined by

$$\varphi^{a,b}(x) = |a|^{-1/2}\varphi\left(\frac{x-b}{a}\right)$$

In wavelet analysis the use of a fully scalable modulated window solves the signal - cutting problem. The window is shifted along the signal and for every position the spectrum is calculated. Then this process is repeated many times with a slightly shorter (or longer) window for every new cycle. In the end the result will be a collection of time-frequency representations of the signal, all with different resolutions. Because of this collection of representations we can speak of a multiresolution analysis. In the case of wavelets we normally do not speak about time-frequency representations but about time-scale representations. Hence, wavelet transform captures both frequency and location information.

A wavelet transform decomposes a signal f(x) using the wavelets $\varphi^{a,b}(x)$ which form a family of real orthonormal bases. The wavelet coefficients are calculated via

$$c_{a,b} = \int_{-\infty}^{+\infty} f(x)\varphi^{a,b}(x)dx$$

& f(x) can be recovered from the wavelet coefficients the formula

$$f(x) = \sum_{m,n} c_{a,b}\varphi^{a,b}(x)$$

When wavelet transform is done in discrete steps, the discrete wavelet

transform is obtained. Every wavelet corresponds with a high and low pass filter. The 2D discrete wavelet transform decomposes the image using high & low pass filters which are applied along horizontal & vertical directions resulting in 4 subimages. Every image can be subsampled by a factor of 2 since half of the frequencies in the subimage have been removed & hence half the samples can be discarded according to Nyquist's rule. This leads to a representation with an equal amount of pixels as the original image. The corresponding 2D filter coefficients can be represented by $A_i=h(k)h(l)$, $H_i=g(k)h(l)$, $V_i=h(k)g(l)$ & $D_i=g(k)g(l)$ where h(k) & g(k) are impulse responses of the lowpass & highpass filters respectively. These coefficients represent different frequency sub-bands & highlight the frequency details at a particular scale. Different wavelet families are used to decompose oral epithelium into multiple sub-bands to analyze detail and coarse level changes in epithelium. Here we have considered basic wavelet called Haar wavelets, Daubechies wavelets. The Haar wavelet operates on data by calculating the sums and differences of adjacent elements. The Haar wavelet operates first on adjacent horizontal elements and then on adjacent vertical elements. One nice feature of the Haar wavelet transform is that the transform is equal to its inverse. The Haar wavelet algorithm has the advantage of being simple to compute and easier to understand. Daubechies wavelets are a family of orthogonal wavelets defining a discrete wavelet transform and characterized by a maximal number of vanishing moments for some given support. In the present analysis, db4 wavelet is used. The Frobenious norm has been computed for H_i, V_i, D_i and A_i and denoted as $\|\bullet\|_F$. The Frobenious norm of $A \in C^{m\times n}$ is defined as

$$\|A\|_F^2 = \sum_{i,j} |a_{ij}|^2 = \sum_i \|A_{i*}\|_2^2 = \sum_j \|A_{j*}\|_2^2 = trace(A^* A)$$

The element of the feature vector (F) is the Frobenious norm of H_i, V_i, D_i and A_i $F = \left[\|H_i\|_F \|V_i\|_F \|D_i\|_F k\|A_i\|_F \right]^T, i = 1,2,3,4$ where k is set as 0.001. k is used to normalize the energy of approximation coefficients(A_i) as its value is quite higher compared to H_i, V_i & D_i.

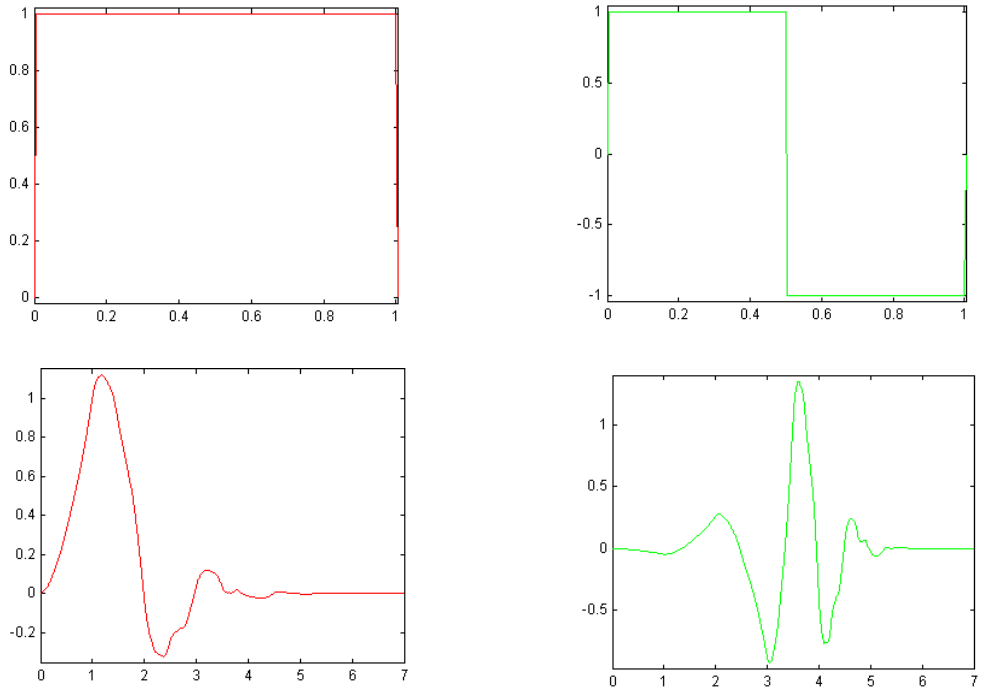

Fig [2.3]. (a) Scaling function φ for Haar & db4 wavelets; (b) wavelet function ψ for Haar & db4 wavelets

2.2 Gabor Wavelets

The human visual system analyzes the textured images by decomposing the image into its frequency and orientation components. Daugman[20] proposed the use of Gabor filters in the modeling of the receptive fields of simple cells in the visual cortex of some mammals. Later Farrokhnia and Jain [21] used it successfully in segmentation and classification of textured images. Gabor filters have some desirable optimality & biological properties. Gabor filters have the ability to perform multi-resolution decomposition due to its localization both in spatial and spatial-frequency domain.

A two dimensional Gabor function is a Gaussian modulated complex sinusoid and it is written as

$$\psi_{i,k}(m,n) = \frac{1}{2\pi\sigma_m\sigma_n}\exp\left(-\frac{1}{2}\left(\frac{m^2}{\sigma_m^2}+\frac{n^2}{\sigma_n^2}\right)+2\pi j\omega m\right)$$

Here, ω is frequency of the sinusoid and σ_m and σ_n are the standard deviations of the Gaussian envelopes. 2-D Gabor wavelets are obtained by dilation and rotation of the mother Gabor wavelet $\psi(m,n)$ using

$$\psi_{i,k}(m,n) = a^{-l}\psi\left[a^{-l}(m\cos\theta+n\sin\theta), a^{-l}(-m\sin\theta+n\cos\theta)\right], a>1$$

where a^{-l} is a scale factor, l and k are integer, the orientation θ is given by $\theta = k\pi/K$, and K is the number of orientations. The parameters σ_m and σ_n are calculated according to the design strategy proposed by Manjunath and Ma [22] which ensures that the half-peak magnitude support of the filter responses in the frequency spectrum touch each other thus reducing the redundancy due to non-orthogonality of Gabor Filters.

$$a = (U_h/U_l)^{\frac{1}{S-1}}, \quad \sigma_u = \frac{(a-1)U_h}{(a+1)\sqrt{2\ln 2}},$$

$$\sigma_v = \tan\left(\frac{\pi}{2k}\right)\left[U_h - 2\ln\left(\frac{\sigma_u^2}{U_h}\right)\right]\left[2\ln 2 - \frac{(2\ln 2)^2\sigma_u^2}{U_h^2}\right]^{-\frac{1}{2}},$$

where U_l and U_h denote the lower and upper center frequencies of interest taken to be 0.1 & 0.4 respectively.

Given an image *I (m,n)*, its Gabor wavelet transform is obtained as

$$x_{l,k}(m,n) = I(m.n) * \psi_{l,k}(m,n) \text{ for } l = 1,2,....,S \text{ and } k = 1,2,....,K$$

where $*$ denotes a convolution operator. The parameters *K* and *S* are number of orientation and number of scales respectively. The mean and the standard deviation are used as features and given by

$$\mu_{l,k}(m,n) = \frac{1}{M^2}\sum_{m=1}^{M}\sum_{n=1}^{N}\left|x_{l,k}(m,n)\right| \text{ and}$$

$$\sigma_{l,k} = \left(\frac{1}{M^2}\sum_{m=1}^{M}\sum_{n=1}^{N}\left(\left|x_{l,k}(m,n)\right| - \mu_{l,k}\right)^2\right)^{\frac{1}{2}}$$

The feature vector is then constructed using $\mu_{l,k}$ and $\sigma_{l,k}$ as feature components, for K = 6 orientations and S = 4 scales, resulting in a feature vector of length 48, given by

$$f = \{\mu_{11}, \sigma_{11}, ..., \mu_{48}, \sigma_{48}\}$$

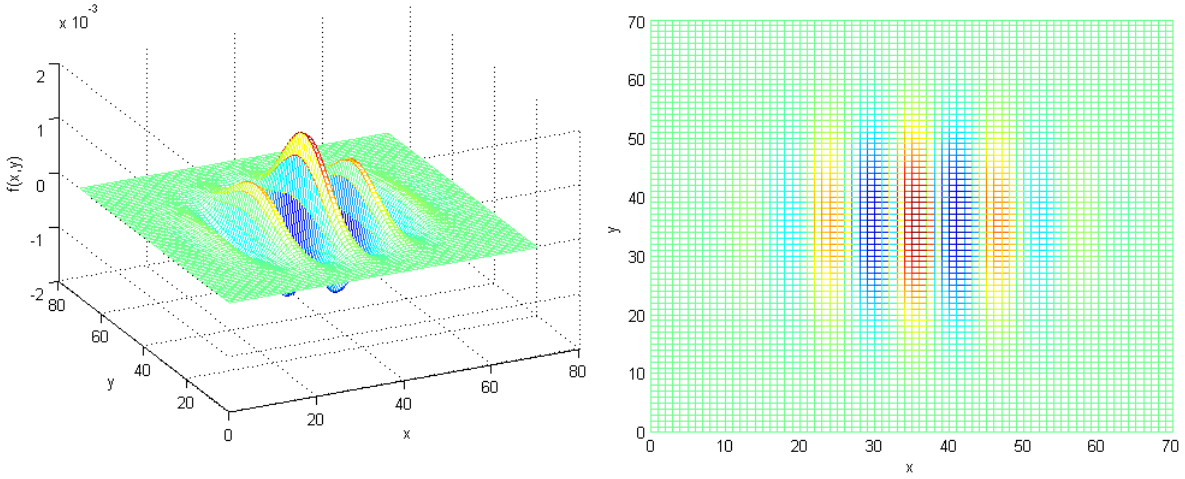

Fig[2.4]Representation of Gabor Filter in spatial domain (frequency=0.15, orientation=90°)

2.2.3. Local Binary Pattern (LBP)

The local binary pattern [23] is a simple and fast method for multi-scale local texture analysis. Since the epithelium tissues are at different orientations within a particular cancer case, rotation invariant texture measure is needed to describe the microstructure following the uniformity criteria. The spatial structure information is combined with contrast which is a measure of the amount of local texture.

Consider a sample neighbourhood from the epithelial layer containing 'P' pixels with g_c corresponding to the gray value of the centre pixel. The texture T for this pixel is given as

$$T = t(g_c, g_0, ..., g_{P-1})$$

where $g_p(p = 0, ...P-1)$ correspond to the gray values of P equally spaced pixels on a circle of radius R that form a circularly symmetric neighbourhood set.

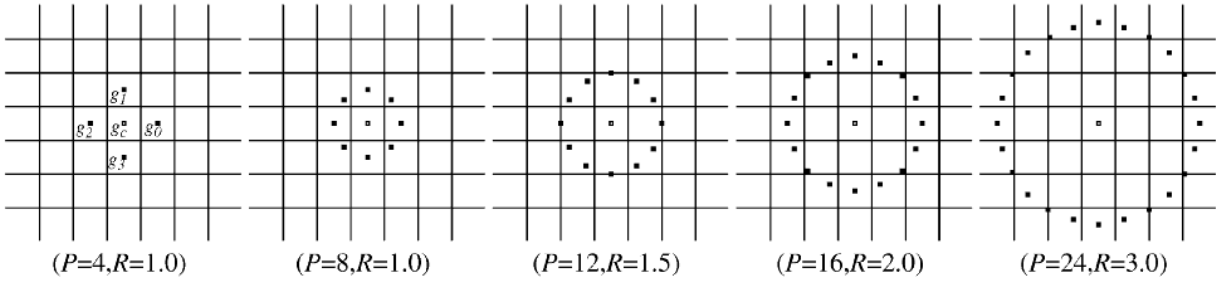

Fig [2.5] Circularly symmetric neighbor sets for different (P, R)

The LBP code for the centre pixel is given as

$$LBP_{P,R} = \sum_{p=0}^{p-1} s(g_p - g_c)2^p$$

where

$$s(x) = \begin{cases} 1, x \geq 0 \\ 0, x < 0 \end{cases}$$

Rotation Invariance is achieved by rotating the neighbor set clockwise such that maximal number of most significant bits is zero in the LBP code.

$$LBP^{ri}_{P,R} = \min \left\{ ROR(LBP_{P,R,i}) \mid i = 0,1....., P-1 \right\}$$

It is observed that certain local binary patterns are fundamental properties of texture, providing the vast majority, sometimes over 90 percent, of all patterns corresponding to radius R present in the observed textures. They have a uniform circular structure that contains very few spatial transitions & function as templates for microstructures such as bright spot (0), flat area or dark spot (8), and edges of varying positive and negative curvature. Hence, to improve the discrimination power of LBP^{ri}, LBP^{riu} using uniformity measure is calculated based on the no. of transitions in the neighborhood pattern. Only patterns with $U \leq 2$ are assigned the LBP code.

$$LBP_{P,R}^{riu2} = \begin{cases} \sum_{p=0}^{p-1} s(g_p - g_c) \text{ if } U(LBP_{P,R}) \\ P+1 \qquad\qquad \text{otherwise,} \end{cases}$$

To include the local image texture contrast, we define a rotation invariant measure of local variance given by:

$$VAR_{P,R} = \frac{1}{P}\sum_{p=0}^{p-1}(g_p - \mu)^2, \text{ where } \mu = \frac{1}{P}\sum_{p=0}^{p-1} g_p$$

The LBP^{riu2} code & local contrast values $VAR_{P,R}$ are computed for 3 radius values; R=8, 16 and 24 with the corresponding pixel count P being 8, 16 and 24 respectively. The mean & variance of each of the LBP output image is calculated which is combined with the mean local contrast of the image to yield 9 LBP features corresponding to each pixel of the epithelium tissue.

2.3 Feature selection by t-test

The 3 textural features are combined to form a feature vector containing 61 features. As the performance of classifiers decrease with the existence of irrelevant and redundant features in the dataset, the necessity for a reduction in dimensionality is essential. Therefore, prior to classification, it is meaningful to verify whether a feature or a set of features has the discriminating capability among the labelled classes or not. In doing so, classical statistical inference provides one of the well-established statistical tests viz., independent samples *t*-test, which is used for comparing the population means of two classes. The t-test is a ratio which assesses whether the means of two groups are *statistically* different from each other. The top part of the ratio is the difference between the two means or averages & the denominator is a measure of the variability or dispersion of the scores. The procedure will also produce confidence interval estimate for the difference of two means. A large difference between the two sample means should lead us to reject the null hypothesis $\mathbf{H}_0$: $\mu_1 = \mu_2$. The p-value is used to determine the likeliness of null hypothesis. The lower the p-value the more "significant" the

result is, in the sense of statistical significance. The 61 features are ranked by their nominal p-value & a set of features falling below a threshold value of 0.05 are considered. The p-values calculated for 61 features are shown in Fig[2.6].As it can be seen, all features are found to be significant.

.

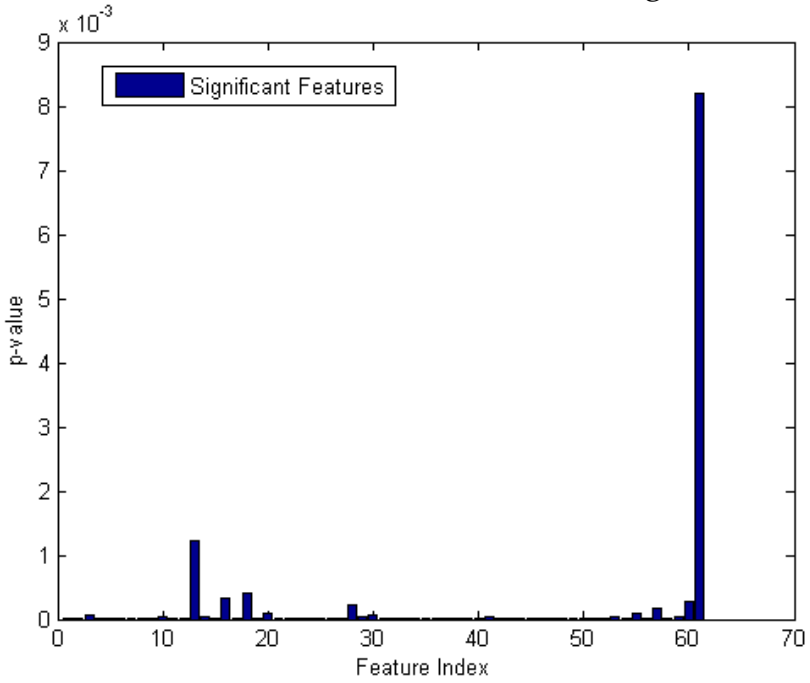

Feature index	Features
1:4	Wavelet energy*
5:13	LBP*
14:61	Gabor wavelet*

Fig [2.6]. Statistical significance of epithelial textural features

2.4 Classification using Support Vector Machines

Recently SVM (Support Vector Machine) has shown many applications in the field of bioinformatics as well as breast cancer classification[24]. SVM is a supervised machine learning method which is based on the statistical learning theory [25]. The SVM algorithm performs a classification by constructing a multidimensional hyperplane that optimally discriminates between two classes by maximizing the margin between two data clusters. When used as a binary classifier, an SVM will construct a hyperplane, which acts as the decision surface between the two classes. This is achieved by maximizing the margin of separation between the hyperplane and those

points nearest to it. The details of the formulation and solution methodology of SVM for binary classification task can be found elsewhere [25].

SVM classification accuracy depends on the penalty parameter and the Kernel Function parameter. In our case penalty parameter was taken to be 5 while the Kernel function was taken to be Radial Basis Functions with gamma=1. To evaluate the robustness of the estimates from the SVM models, a 3-fold cross-validation was performed in the training data set. The training data set was partitioned into 3 equal-size subsets. Each subset was used as a test data set for a model trained on all cases and an equal number of non-cases randomly selected from the 2 remaining data subsets. This cross-validation process was repeated 3 times, allowing each subset to serve once as the test data set. To generate summary performance estimates, we averaged sensitivity, specificity & accuracy of the cross-validations. **S**ensitivity and specificity of the classifier are defined as:

$$\text{Sensitivity} = \frac{TP}{TP + FN} \quad \%$$

$$\text{Specificity} = \frac{TN}{FP + TN} \quad \%$$

where

TP: True Positive: Case predicted with OSF when it actually has oral cancer.

TN: True Negative: Case predicted normal when it actually is normal.

FP: False Positive: Case predicted with OSF when it actually is normal.

FN: False Negative: Case predicted normal when it actually has oral cancer.

Sensitivity is thus a measure of accuracy of diagnosis of malignant (true) cases of OSF. Specificity is a measure of accuracy of diagnosis of benign (false) cases of OSF. The overall accuracy, specificity and sensitivity of the classifier have been shown in Table 3.1.

Feature set	Fold #1	Fold #2	Fold #3	Net value
Accuracy				
Db4+Gabor Wavelet+LBP	93.93939	87.87879	90.90909	90.90909
Haar+Gabor Wavelet+LBP	93.93939	78.78788	96.9697	89.89899
Specificity				
Db4+Gabor Wavelet+LBP	90.90909	80	83.33333	84.74747
Haar+Gabor Wavelet+LBP	84.61538	63.63636	91.66667	79.9728
Sensitivity				
Db4+Gabor Wavelet+LBP	95.45455	91.30435	95.2381	93.999
Haar+Gabor Wavelet+LBP	100	86.36364	100	95.45455

Table [2.1] Accuracy, Specificity & Senstivity of SVM using features Gabor Wavelets, LBP & db4/Haar wavelets

CHAPTER THREE

Improved Segmentation of Epithelial Layer

In Chapter two, the Otsu Thresholding based segmentation of the epithelial layer leads to redundant edge pixels being attached to the epithelial layer resulting from the individual cell boundaries inside the epithelium and sub-epithelial layers. Methods such as Otsu thresholding are rudimentary similarity based methods as it is based on the intensity comparisons between pixels and regions. The interface between two different contiguous homogenous regions is usually marked by a discontinuity in gray-level, color, or texture. Segmentation can therefore be based on the detection of such discontinuities. More sophisticated similarity based methods include the so called split and merge and clustering techniques in order to partition pixels within a defined feature space. The watershed transformation is a technique for segmenting digital images that uses a type of region growing method based on an image gradient. It thus effectively combines elements from both the discontinuity and similarity methods. Since epithelial images contain textured regions, the necessary smoothing that is essential in gradient extraction has the effect of removing texture information. In order to improve watershed techniques and apply them properly to textured epithelial images, the texture content information that is removed should be included.

This chapter presents a straightforward extension of the watershed algorithm to make use of information in all texture channels. In the technique proposed, several texture channels are computed from the preprocessed original image. A vector gradient is used to compute the edge of the multichannel image. The vector gradient is combined with the intensity gradient yielding the final gradient image. After an automatic selection of significant minima, a watershed transform is applied. Finally, a multivariate region merging step using color, histogram matching and texture based criterion is carried out to obtain the final segmentation. The complete segmentation procedure consists on the following steps & is shown in Fig [3.1]

- *Pre-Processing:* Wiener filtering & contrast enhancement
- *Texture analysis:* A set of *n* channels is obtained from the original image by computing *n* texture features on every pixel.
- *Gradient computation:* Considering each point of the image as an *n*-valued vector, a gradient image is obtained by computing the gradient of the vector field & is combined with intensity gradient.
- *Minima selection:* According to some measure, local minima are selected from which the watershed process will begin.
- *Watershed segmentation:* Starting from the selected minima, the image is flooded by extending their zone of influence in higher gray levels. When two regions come into contact a watershed line is erected.
- *Region merging:* Watershed regions are iteratively merged, according to a similarity criterion using colour & texture, to obtain the final segmentation.

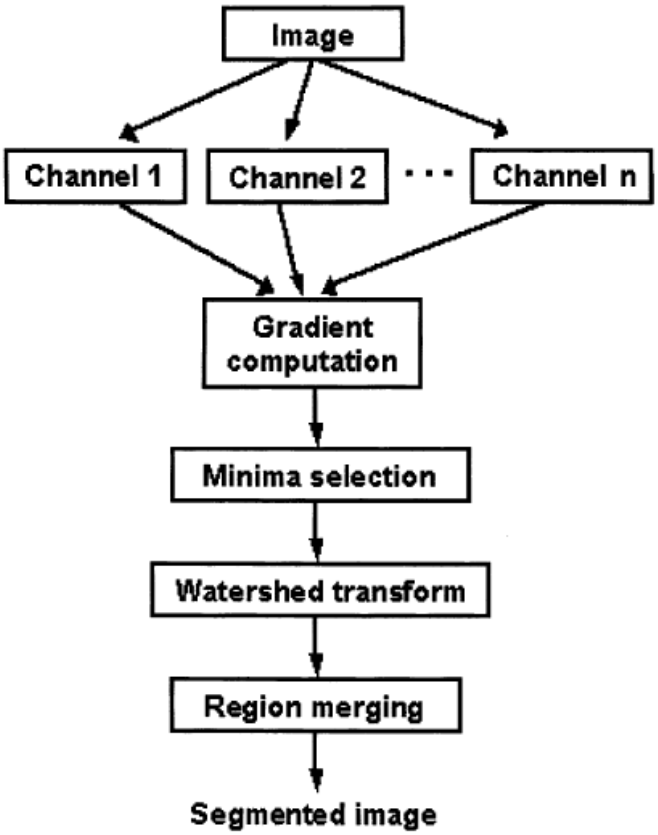

Fig [3.1] Overall diagram of texture gradient based epithelial layer segmentation

3.1 Pre-Processing

Since the epithelial images contain noise & staining variations, a pre-processing step consisting of the following operations is applied:

- Filtering the RGB image by a 5x5 wiener filter to reduce the noise.
- Adjusting the RGB image intensity values using Contrast Limited Adaptive Histogram Equalization.

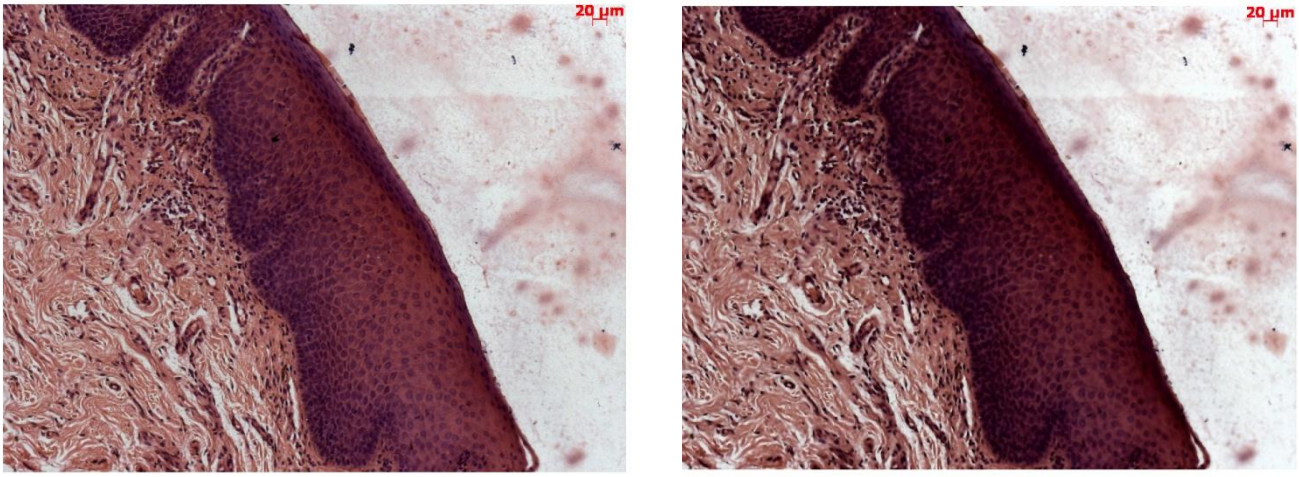

Fig [3.2] Pre-processing of epithelial image (a) Original RGB image (b) Preprocessed image

3.2 Texture Characterization

In order to produce a texture gradient we first need to characterise the texture content of the image at each pixel. **A** number of methods have been proposed to do this. One of the most popular techniques is the use of a set of differently scaled and orientated complex Gabor filters .By suitable spanning of the frequency space, each pixel can be characterised in texture content. We make use of the Gabor filter design proposed by Jain & Farrokhnia [21]. Gray level intensity image (I(x,y)) is computed from the processed RGB image & is passed through a bank of Gabor filters, and a set of filtered images $I_{mn}(x,y)$ are obtained. In our work, we choose 6 orientations, namely, n = 0,1,2,3,4,5 corresponding to the orientations: 0°, 30°,60°,90°,120° and 150° and 4 scales namely, m=0,1,2,3 corresponding to frequencies $\frac{\sqrt{2}}{4}, \frac{\sqrt{2}}{8}, \frac{\sqrt{2}}{16}, \frac{\sqrt{2}}{32}$. Using the rotation and scaling of the base filter g(x, y), we get the bank of Gabor filters $g_{mn}(x,y)$ for decomposing the input image. To make sure that the filters don't

respond to regions with constant intensities (DC components), we set $G_{mn}(0,0) = 0$, where $G_{mn}(u,v)$ denotes the Fourier transform of $g_{mn}(x, y)$. $I_{mn}(x, y)$ is the modulus of the convolution of the input image I(x, y) with Gabor filter $g_{mn}(x, y)$.

$$I_{mn}(x,y) = | I(x,y) * g_{mn}(x,y) |$$

where *m*= 0,1,2,3 & n = 0,1,2,3,4,5 and * denotes the convolution operator in two dimensions. Each filtered image is subjected to a Gaussian with $\sigma=2*\sigma_g$ (sigma of Gabor Filter) to smoothen the textural information. As a result, for an input image there are totally 24 output images associated with the bank of 24 Gabor filters, denoted by $I_{00}(x,y)$, $I_{01}(x,y)$ ….. $I_{35}(x\ y)$.

3.3 Computation of Gradient Image

To apply edge based segmentation algorithms to multichannel data, a gradient of the multichannel image must be defined. Instead of separately computing the scalar gradient for each channel, the vector gradient proposed by DiZenzo [26] is used to detect boundaries in multidimensional images. This is because when the attribute components are highly correlated, vector gradients are less sensitive to noise than the sum of the squares of scalar gradients in each channel. A multichannel image can be seen as a vector field f: S » R^m, defined on a subset S of R^n. Let f_k denote the kth component of f. It can be proved that the first-order Taylor expansion takes the form

$$f(x+a) = f(x) + [f'(x)](a) + ||a||e(x,a)$$

where e(x,a)→ 0 as a→ 0 and f′(x) is now an m x n Jacobian matrix D(x):

$$f'(x)=D(x) = \begin{pmatrix} D_1 f_1(x) & \cdots & D_n f_1(x) \\ \vdots & \ddots & \vdots \\ D_1 f_m(x) & \cdots & D_n f_m(x) \end{pmatrix}$$

being $D_j f_k$ the first partial derivative of the k^{th} component of f with respect to the j^{th} component of x.

According to Cumani[27],the extrema of D(x) are obtained in the directions of its eigenvectors θ_+ & θ_- the values attained there are the corresponding eigenvalues λ_+ and λ_- .The approximation of edge for vector

values image is obtained as TG(x,y) = λ_+ -- λ_- .Fig[3.3b] shows the image of texture gradient computed for a case & it clearly highlights the edge of the cellular textured region.

To include the intensity information, the texture gradient is combined with an intensity gradient as follows

$$G(x,y) = mix * \nabla(I(x,y) + TG(x,y)$$

where mix is chosen to be 0.5.The processed RGB image is transformed to L*a*b color space & the intensity gradient is calculated by summing up the gradients for L, a & b channels. L*a*b color space is used because the three channels are very less correlated as compared to RGB space. The final gradient image G(x,y) is shown in Fig[3.3c]

3.4 Minima Selection & Watershed Segmentation

The watershed transform is the main segmentation technique in mathematical morphology. It has been applied successfully to 2D [28]as well as to 3D images [29]. It is a connected (it divides the image into sets of connected pixels) and complete (it assigns every pixel to one of the classes) method. In a topographic surface, the watersheds are the lines dividing two catchment basins. Each basin is associated to a local minimum & the whole region is flooded with water. Starting from every minimum, the surface is progressively flooded until water coming from two different minima meet thus segmenting the region into separate closed & connected regions. This is the main advantage over traditional edge based techniques which most often form disconnected boundaries that need post-processing to produce closed regions. We have used four neighbour connectivity for watersheds in the algorithm. The main disadvantage is that since the transform starts from every minimum, the result excessive over-segmentation. Hence a minima selection procedure based on dynamics followed by region merging is used to merge similar regions.

The dynamics algorithm is applied to the gradient of the image for minima reduction. Dynamics provides an intuitive selection scheme controlled by a single parameter. The deepness of a basin would be the level the water would reach, coming in through the minimum of the basin, before the water would overflow into a neighbour basin. The dynamics of a basin is a similar concept, but referring to a neighbour basin with a lower minimum than the actual one. It is computed using morphological reconstruction [30]. Given two gray-scale images f and g, where g is smaller than or equal to f in all points, the morphological reconstruction by erosion of f over g is the result of the following iterative procedure as follows:

$$f_{k-1}(p) = \max(g(p), f_k(p)\Theta B)$$

where Θ denotes the gray-level erosion of the function using a structuring element B.

It can be proved that if the morphological reconstruction [30] of the image g from an image f=g+d is computed, the resulting function will have a watershed transform in which the regions with dynamics lower than d (minima selection threshold), have been eliminated. The value of the dynamics is taken to be 20.The result of the minima selection is shown in Fig [3.3d].The labelled image obtained after gradient based watershed segmentation of the image is shown in Fig[3.3e]

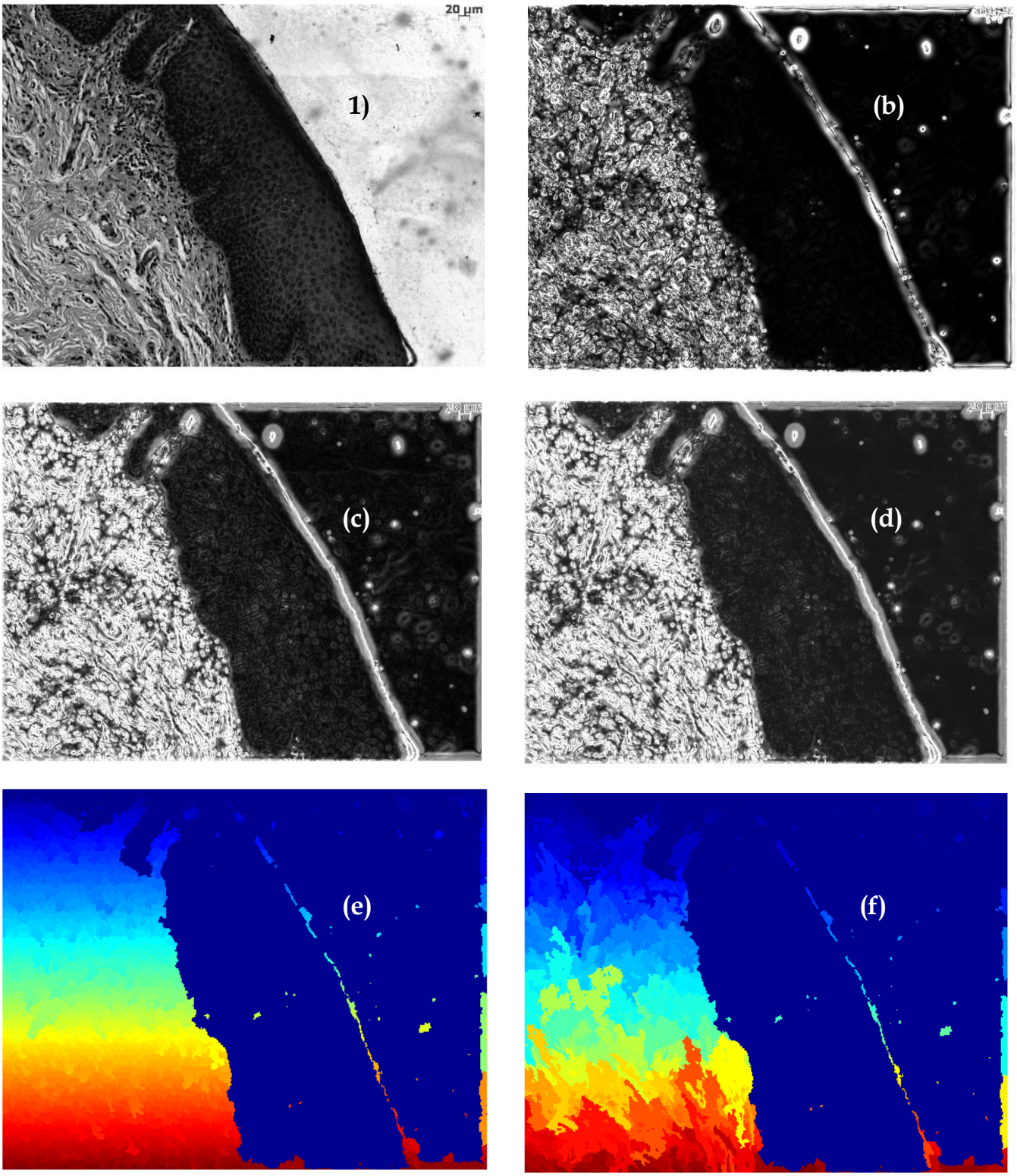

Fig [3.3](a)Original intensity image(b)Texture gradient image (c)Intensity + Texture gradient image(d)Gradient image after minima selection (e)Watershed segmentation (f)Result of first region merging step

3.5 Multivariate Region Merging

To obtain the final segmentation, regions resulting from the watershed need to be merged to segment the epithelial layer. The region merging is a two-step procedure described as follows

1) In the first step, all regions resulting from the watershed transform are ordered into a region adjacency graph (RAG) in which nodes correspond to regions and arcs to the frontier between two regions. Initially only smaller regions with area<100000 are merged using color based Hotelling T^2 Test criteria. The Hotelling criteria states that assuming a multivariate normal distribution of gray levels in a region, we can apply Hotelling's T^2 test to compare the means of two populations. The applied statistic is given by:

$$T^2 = (\mu_1 - \mu_2)^T \left[\sqrt{\frac{1}{n1} + \frac{1}{n2}}\, S \right]^{-1} (\mu_1 - \mu_2)$$

where μ_1 and μ_2 are the vector means of each region, respectively, and *S* is a pooled covariance matrix of the form:

$$S = \sqrt{\frac{n1 * \sigma 1 + n2 * \sigma 2}{n1 + n2}}$$

σ_1 and σ_2 being the covariance matrices of each region. The T^2 value is calculated on the processed RGB image and its threshold value is taken to be 300. The result is shown in Fig [3.3f].

2) The second step consists of merging the regions based on similarity measure defined using intensity difference, histogram difference & texture energy. The parameters are described as follows:

- *Intensity difference:* The difference on the mean value of the intensities in the two regions is computed as follows:

$$Diff = \sum_{j=1}^{n} \sqrt{(\mu_1 - \mu_2)}$$

The threshold value for intensity difference is taken to be 0.01 & is used in conjunction with the next 2 criteria.

- *Histogram difference:* Intensity histograms are calculated for each region using the gray level image. Once intensity histograms have been calculated, the histogram distance between each pair of neighboring regions is measured as

$$X^2\left(H_{R_i}, H_{R_j}\right) = \sum_b \frac{\left(H_{R_i}(b) - H_{R_j}(b)\right)^2}{\left(H_{R_i}(b) + H_{R_j}(b)\right)}$$

$$\forall R_i, R_j \in P_1,$$

where P_1 is the set of all pairs of neighboring regions (R_i,R_j) in the first frame, H_{Ri} and H_{Rj} are the histograms of R_i and R_j, and b is the histogram bin. After the distances have been calculated, all neighboring regions satisfying X^2<0.2 are merged.

- *Texture difference:* For filtered image $I_{mn}(x,y)$, we define a window $W_{mn}(x,y)$ of size w x w, centered at pixel (x,y) to capture the local texture characteristics. Associated with pixel I(x,y), a histogram $f_{mn}(x,y,t_k)$ is computed by

$$f_{mn}(x, y, t_k) = \sum_{(x',y') \in W_{mn}(x,y)} \delta(I_{mn}(x', y') \in (t_{k-1}, t_k))$$

where δ(.) takes the value one when the condition inside is satisfied; zero otherwise. t_k is an appropriate binning, and k = 1,2 ... K. K is the maximum number of bins. Let η be a certain neighboring structure. Corresponding to the $(m,n)^{th}$ Gabor channel, $H_{mn}(x,y)$ denotes the proximity (similarity) measure between pixel (x,y) and its neighbours according to η in $I_{mn}(x, y)$, and it is computed by: $H_{mn}(x, y) = \sum_{(x',y') \in \eta} \sum_{k=1}^{K} | f_{mn}(x, y, t_k) - f_{mn}(x', y', t_k) |$

The 4-nearest neighbourhood is taken in this method. To judge the similarity of adjacent pixels the measure defined by Minkowski norm is

used calculated as $H_{sum}(x,y) = \left(\sum_{m=0}^{2} \sum_{n=1}^{3} (H_{mn}(x,y))^{p} \right)^{\frac{1}{p}}$ where p is taken to be 2. Pixels with same texture have smaller values of $H_{sum}(x,y)$ while pixels near a boundary have large $H_{sum}(x,y)$ values. A low pass filter is applied on $H_{sum}(x,y)$ image to smoothen it & a merging threshold of 0.04 is taken for H_{sum} difference.

The region merging is continued until no further regions are merged together and region below a certain area (500) are ignored as they are considered to be due to noise. The final labeled image obtained is shown in Fig.[3.4a] while the $H_{sum}(x,y)$ image is shown in Fig[3.4b]

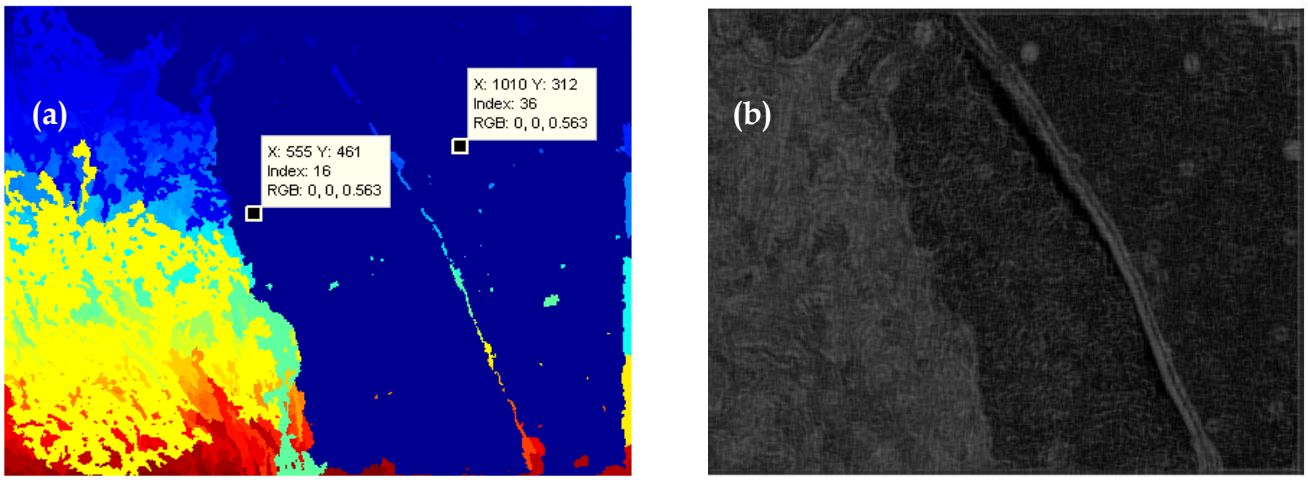

Fig [3.4] (a) Labeled image after multivariate region merging (b) $H_{sum}(x,y)$ image

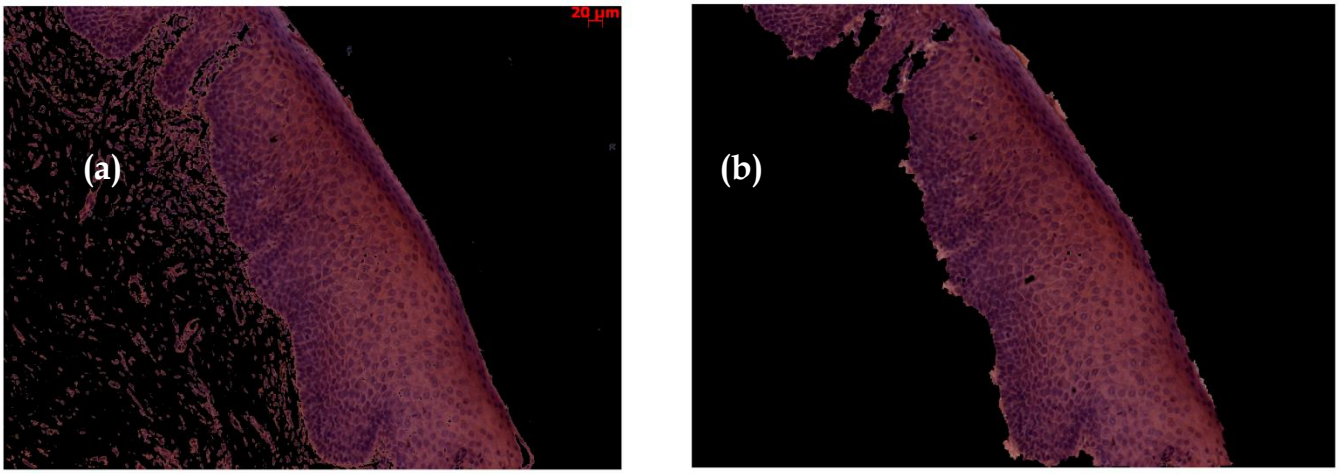

Fig [3.5] (a) Otsu thresholding result (b) Improved segmentation of epithelial layer

3.6 Results for other cases and comparison with Otsu thresholding

Texture gradient based watershed Otsu thresholding

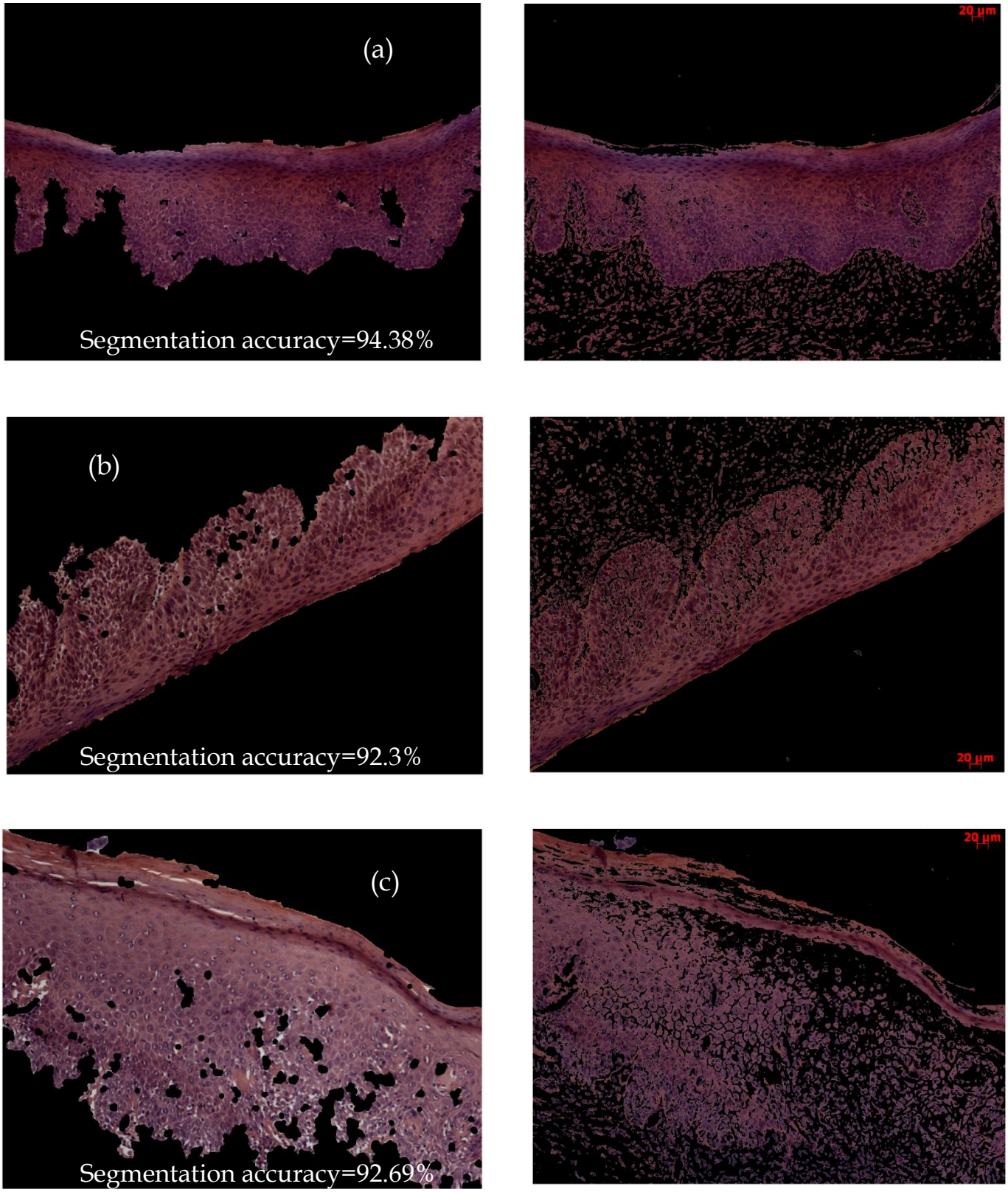

CHAPTER FOUR

Cell Segmentation and Analysis

Segmentation of epithelial cells is crucial for analysis of histological images. Generally, basal cells form the proliferative compartment of the epithelium from which cells migrate, differentiate as they progress and eventually desquamated at the surface. The keratinocytes of the basal cell layer of the oral stratified squamous epithelium represent the progenitor cells that are responsible for the production of other cells making the various layers of the epithelium. Changes in the basal cells may have serious implications on future cell behavior, including malignant transformation.

The Oral Mucosa basal cell segmentation is one of the most difficult segmentation among different types of cell images. This is because of its diversity in the structures and the overlapped cell clusters. The major features of malignancy are related with the nuclei of the cells. Normally, nucleus shape is small and almost round. Its intensity is darker than cytoplasm. Malignant or pre-cancerous cells have larger and darker nuclei and tend to cling together in clusters. Also malignancy results in greater intensity variations within the cell. The measurement of their size and shape in OSF may be an important prognostic marker as studies have shown that there is an increase in the size and shape of both the cell and the nucleus during OSF. It is therefore essential to operate a segmentation of the image, to isolate the cells from the rest of the image. The watershed transform[33] has proven to be a powerful and fast technique for both contour detection and region-based segmentation. It is simple and intuitive, can be parallelized, and always produces an entire partition of the image. Watershed segmentation often results in over-segmentation due to intensity variations within both objects and background. Seeded watersheds, where the number of segmentation boundaries is limited to a set of input seeding regions, have been used for segmentation of cell nuclei in images produce by fluorescence microscopy. Fully automatic seeding often results in

more than one seed per object, or objects containing no seed at all. To improve the segmentation, the segmentation and tracking can be combined. A popular method that combines the segmentation and tracking is active contours (snakes), previously used for cell segmentation/tracking in e.g. [32].

Appropriate merging techniques have been devised based on the cell features like circularity, binding energy etc. for correcting the oversegmentation done by watershed. The initialization step of the process is probably the most critical step of this kind of transform. A good set of markers will avoid severe over-segmentation. The initial boundaries obtained from watershed segmentation are used as initialization contours for GVF snake which tracks the boundary of the cells thus segmenting the final cell.

4.1 Initial Seeding & Watershed segmentation

H & E deconvolution is applied on the RGB basal cell image to remove the color due to staining. As the image intensities of the cells show a range of values partly overlapping with the background intensities, intensity thresholding will not separate cells from background in a satisfactory way. A more effective method for separating objects from background is using variance measures. Object seeds at the initial step are found using the extended h-maxima transform that filters out local maxima using a contrast criterion. All maxima with heights smaller than a threshold level h are suppressed. We take a lower value of h=15 since the merging step below compensates for oversegmentation. All foreground seeds are uniquely labeled using connected component labeling. The seeds obtained from the h-maxima transform are then combined with the thresholded image to obtain the final seed points.

The object seed information is used as input for watershed segmentation. Seeded watershed segmentation is applied to the inverse of the original intensity image. The dark edges of the cells are thus interpreted as ridges, and the brighter cells and background as shallow valleys in the

watershed landscape. Seeds represent holes in the landscape, and as the landscape is submerged in water, the water will start to flow into the minima of the landscape, creating one catchment basin associated with each local minima. As the water rises, water from neighboring catchment basins will meet. At every point where two catchment basins meet, a dam, or watershed is built. These watersheds are the segmentation of the image. The watershed image is combined with the thresholded image of the cells to obtain final segmentation. The initial result of seeded watershed segmentation of Fig 4.2(a) using the seeds from Fig 4.2(c) is shown in Fig 4.2(d)

4.2 Cell contour tracking using GVF snakes

The watershed segmentation gives the initial boundary around a cell which also contains the background epithelial region. To segment the exact boundaries of objects, we use an energy-minimizing contour, called "snake" [33], which is guided by external constraint forces and influenced by images forces that pull it toward the edges. Snake provides a powerful interactive tool for image segmentation. We use the contour obtained from the previous segmentation result as the initial contour, and then move this contour close to the more accurate cell contour under the influence of internal forces depending on the intrinsic properties of the curve and external forces derived from the image edge data.

To obtain good segmentation result, Gaussian Blur is applied on the image which restrains the noise in the cell image. The edge gradient of the image is computed using edge computation by Sobel operator. Flexible parameter α and rigid parameter β are also analysed by testing it one different cases, which prove that the snake model cannot get good convergence result if α is less than 1.Hence α is taken to be 1.2. Furthermore, parameter β doesn't work in any cases. At the same time, iteration times of GVF Snake are analysed too. The segmentation result becomes stable if the iteration times for gradient computation is bigger than 80 in these cases. Fig [4.1] shows an

example of a cell being tracked by the GVF snake. The red lines indicate the moving contour at different points of time

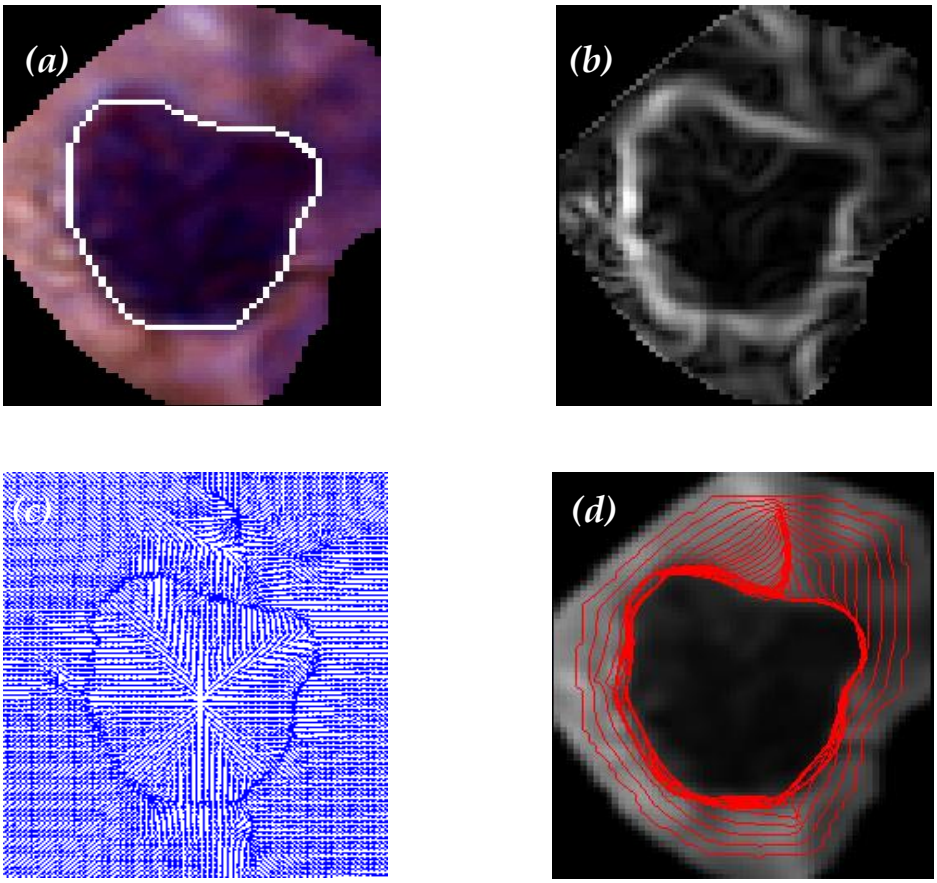

Fig [4.1] (a) Final contour obtained using GVF (b) Gradient image (c) Normalized GVF field (d) Deformation of the contour

4.3 Merging of fragments

Watershed segmentation often results in over-segmentation of some cells. The fragments of a cell tracked by GVF therefore need to be merged together. The guiding factor for making these merging decisions is a 2D mathematical model of the nuclei based on a combination of morphometric features, which includes area, convexity, shape factor, and bending energy.

4.4 Features for Object Modeling

Area: The area (size) of the object, A, is the total number of pixels in the

object.

Convexity: The convexity, denoted C, of an object is the ratio of the object area to the area of the convex hull of the object. The convex hull of an object is formed by the well-known Jarvis March algorithm (54). The convexity is typically close to 1 for circular and elliptical objects and less than 1 for concave objects.

Shape factor: Let P denote the perimeter and A the area of an object. The shape factor denoted by U is defined as

$$U = \frac{P^2}{4\pi A}$$

Bending energy: The boundary pixels of the 2D object are denoted $(x_0,y_0),(x_1,y_1)\ldots..(x_{n-1},y_{n-1})$.The bending energy , E is defined as

$$E = \frac{1}{n}\left(\sum_{i=1}^{n-1} \theta_{i+1} - \theta_i)\right)^2$$

$$where\ \theta_i = \tan^{-1}\left(\frac{y_{i+1} - y_i}{x_{i+1} - x_i}\right)$$

The reason to use 2D bending energy is its simplicity and lower computation cost. With the above-defined features, the feature vector for an object is simply **f** = (V, C, U, E). This feature set was found to be effective yet minimal for these data.

The score of a fragment is formulated as:

$$S = (A - A') + C - U - E$$

where A' denotes the approximate area of the nuclei calculated in advance. The proposed score captures the intuition that, compared with the fragments of nuclei, a correctly formed nucleus tends to have (a) an appropriate area A, (b) high convexity C, (c) low shape factor U , and (d) low bending energy E.

The fragments are combined only if the final score of the combined structure is greater than the score of each of the individual fragments.

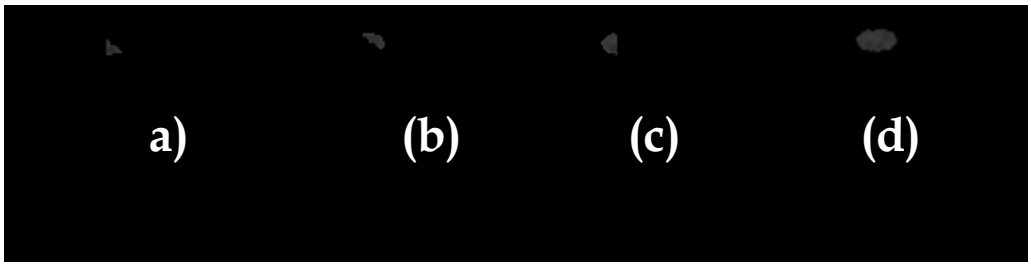

Fig [4.2] Fragments formed due to oversegmentation are combined to form a cell (a) Score=-1.7423 (b) Score=-4.05 (c) Score=-9.40 (d) Score=-1.2643

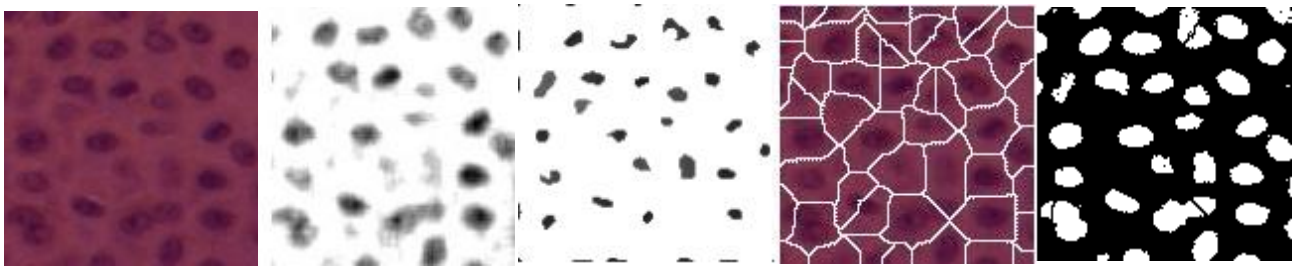

(a) (b) (c) (d) (e)

Fig [4.3](a) Epithelium layer sample(b) Deconvoluted image (c) Initial seeds for watershed (d) Result of watershed transform (e)Finally segmented cells

Fig[4.4] Some cell contours tracked using GVF based snakes

4.5 Feature Extraction

Let P, A, W, H denote the perimeter, area, width (major axis length), height (minor axis length) of the cell nucleus respectively. To analyze the segmented cells from the epithelial layer, following properties are computed for each cell nuclei:

1. *Nuclear Area (f_1)*
2. *Nuclear Perimeter (f_2)*
3. *Rectangularity of the cell region (f_3):* $R = A/(W \times H)$

   W stands for the width, H stands for the height. R describes the deviation degree of the cell to the rectangle.
4. *Compactness (f_4):* $U = \frac{P^2}{4\pi A}$
5. *Convex area (f_5):* Area of the convex hull (area of the smallest convex set of pixels containing the entire nuclear object)
6. *Solidity (f_6):* Nuclear area divided by the area of the convex hull
7. *Roundness (f_7):* Nuclear area divided by the area of a circle with diameter equal to the length of the major axis.
8. *Eccentricity (f_8):* Eccentricity of the ellipse that has the same second-moments as the nuclear region i.e. e=$\sqrt{1 - \frac{W^2}{H^2}}$
9. *Concavity (f_9):* Convex Area-Nuclear Area
10. *Orientation (f_{10}):* Angle (in degrees) between the x-axis and the major axis of the ellipse that has the same second-moments as the region.
11. *Area Irregularity (f_{11}):* The nucleus is rotated so that its major axis becomes horizontal & is then enclosed by a minimum bounding rectangle (MBR). There is at least one intersecting point between a nucleus and each side of its MBR as shown in Fig. [4.5]. If there are two or more intersecting points at one side, the middle one is selected as the representative intersecting point. Then, a nucleus is partitioned into four parts as follows. If an intersecting point is on a vertical side of the MBR, a horizontal cutting line will go through this point. If an intersecting point is on a horizontal side of the MBR, a vertical cutting line will go through this point. Consequently, four possibly

overlapping areas S1, S2, S3, and S4 will be formed with each area surrounded by a segment of nucleus's boundary, a vertical line, and a horizontal line. The area irregularity is given as

$$f_{11} = \frac{1}{4}\sum_{j=1}^{4} \max_{k=1...4, k\neq j} \left| \left|S_j^i\right| - \left|S_k^i\right| \right|$$

12. *Contour irregularity (f_{12}):* The contour of the nucleus can be represented by a sequence of k equal spacing sample boundary points $\{p_0\ p_1\ p_2 \ldots\ldots p_{j-1} p_j \ldots\ldots p_{k-1}\}$ with $p_k = p_0$ and $p_{-1} = p_{k-1}$. Let $p_j(w)$ be the boundary point with a distance of w pixels from the current point p_j. The curvature at point p_j is defined as:

$$d_j^i = \tan^{-1}\frac{y_j - y_j(w)}{x_j - x_j(w)} - \tan^{-1}\frac{y_{j-1} - y_{j-1}(w)}{x_{j-1} - x_{j-1}(w)}, d_{-1}^i = d_{k-1}^i$$

Therefore, contour irregularity is defined as

$$f_{12} = \frac{1}{k}\left(\sum_{j=0}^{k-1} |d_j^i - d_{j-1}^i|\right)$$

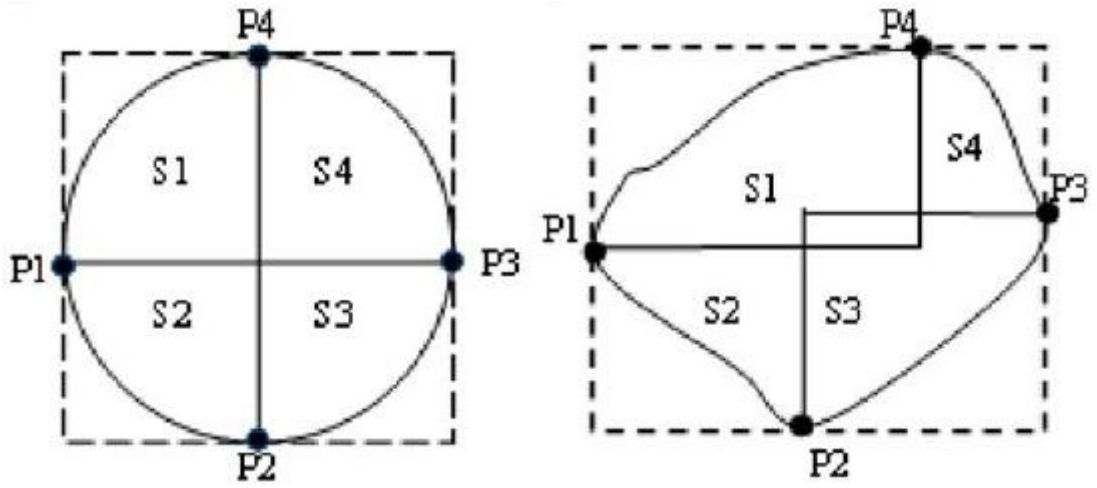

Fig [4.5] Area irregularity (a) Round nucleus (b) Irregular nucleus

13. *Spot areas ratio (f_{13}):* Pigmentation is an important characteristic appearing in a malignant tumor. In our system, the bright and dark spots can be detected by top-hat and bottom-hat transforms, respectively, on nuclei using a disk shape structuring element of radius 5. Top-hat transform is the difference between an input image and its opening by some structuring element, and

bottom-hat transform is the difference between the closing and the input image. Top-hat transform returns an image containing elements that are smaller than the structuring element and brighter than their surroundings. Bottom-hat transform returns an image containing elements that are smaller than the structuring elements and darker than their surroundings.

$$f_{13} = \frac{1}{n}\sum_{i=1}^{n}\left(\frac{1}{||N_i||}(||B(N_i)|| + ||D(N_i)||)\right.$$

14. *Texture features (f_{14}-f_{17}):* Haralick's texture features [34] were calculated using the gray-level co-occurrence matrix. This matrix is square with dimension N_g, where N_g is the number of gray levels in the image. Element [*i,j*] of the matrix is generated by counting the number of times a pixel with value *i* is adjacent to a pixel with value *j* and then dividing the entire matrix by the total number of such comparisons made. Each entry is therefore considered to be the probability that a pixel with value *i* will be found adjacent to a pixel of value *j*.4 statistics namely contrast, correlation, homogeneity & energy are calculated from the co-occurrence matrices calculated using offsets as (1,0);(-1,0);(0,1);(0,-1).Thus

f_{14}-f_{17} = {Contrast (GLCM), Homogeneity (GLCM), Energy (GLCM), Corr(GLCM)}

15. *Mean intensity of the nucleus (f_{18}):*

These all features are concatenated to form a feature vector of length 18.The cell dataset consists of 886 & 809 cell samples for normal & OSF cases respectively.

4.6 Feature Ranking & Classification

The 17 features are ranked using an F-score calculated as:

$$F_i = \frac{(\bar{x}_i^{(+)} - \bar{x}_i)^2 + (\bar{x}_i^{(-)} - \bar{x}_i)^2}{\frac{1}{n_+ - 1}\sum_{k=1}^{n_+}(x_{k,i}^{(+)} - \bar{x}_i^{(+)})^2 + \frac{1}{n_- - 1}\sum_{k=1}^{n_-}(x_{k,i}^{(-)} - \bar{x}_i^{(-)})^2},$$

X_i, $X_i^{(+)}$ & $X_i^{(-)}$ are average of feature i for whole, positive & negative datasets.

t-test is used to find the relevant features as described in section 2.4. The 18 features are ranked by their nominal p-value & a set of features falling below a threshold value of 0.05 are considered to be useful for classification. The F-scores & p values for the 18 features are plotted below:

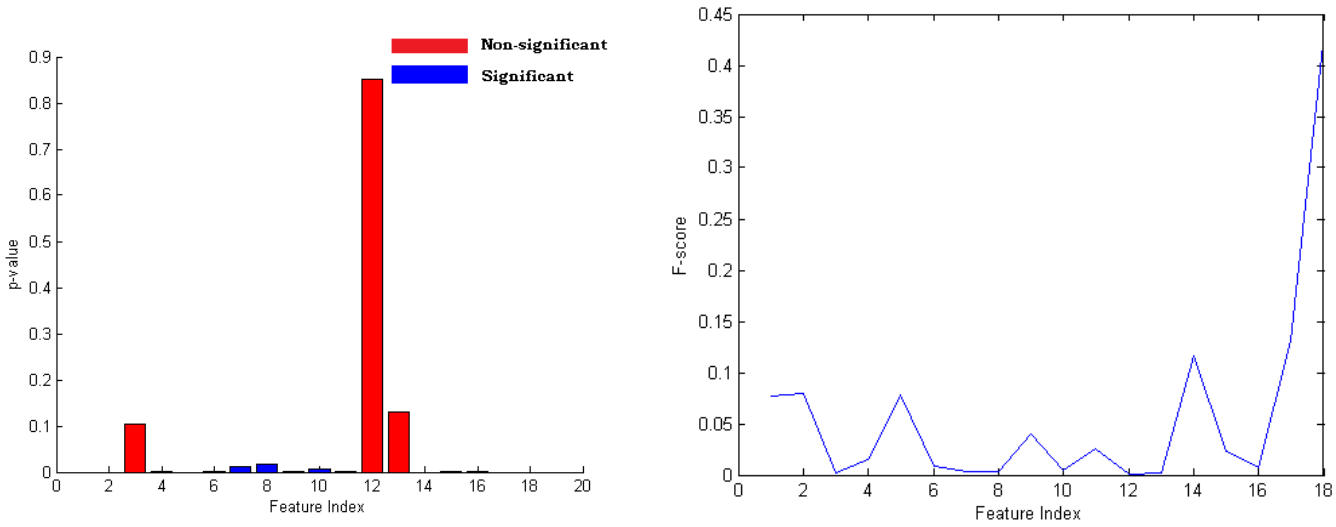

Fig [4.6]Plots showing F-score & p values for nuclear feature indices

Features 3, 12 & 13 corresponding to rectangularity, Contour irregularity & Spot areas ratio are dropped because their p values are greater than 0.05.The remaining feature vectors are subjected to 3 fold cross validation & fed to a classifier based on Radial basis SVM(gamma=1) and following results are obtained:

	Fold#1	**Fold#2**	**Fold#3**	**Net Value**
Accuracy	79.09	80.89	82.15	80.71
Specificity	81.37	80.25	77.05	79.55
Selectivity	79.99	82.49	80.56	81.01

CHAPTER FIVE

Conclusions

In this thesis, a new attempt has been made to analyze the texture of epithelial tissue for detection of OSF & no approach has been made to make use of textural features till date. Multi-scale feature extraction techniques are not only used, but also compared for achieving to an optimal subset of textural feature space leading to higher accuracy. It is observed through detailed statistical analysis that all 61 textural features are statistically significant thus supporting the texture approach. A simple support vector machine based classifier is trained with the labeled samples based on the complete feature space & leads to a diagnostic accuracy of 90.9% wherein texture features are used along with db4 wavelet family. It can be concluded that certain selected texture measures play a complementary role to each other in the process of quantitative texture characterization pertaining to cancer detection.

The texture gradient based watershed segmentation is found to be quite successful as compared to Otsu thresholding based segmentation and its accuracy has been found to be ranging from 80% in OSF images to 96% in normal images. This accuracy has been calculated by comparing with the ground truth images generated by the medical experts. Since watershed always leads to formation of closed contours, the redundant cells attached to the epithelial layers are removed in that case. Also intensity variations are taken care of since we take into account the texture information also. This is clearly validated in Section3.6 (Fig c) where Otsu thresholding leads to big holes within the epithelial layer while the watershed segmentation segments out the epithelial layer completely.

In cell segmentation, the GVF based snake is used for cell contour extraction rather than the conventional classical snake as it solves the problem of converging to a local minimum in case the contours are initialized from the region of interest. Since the watershed contours are of arbitrary shape, GVF snake is found to be more robust. However in some cases GVF snake fails to track the cell and goes within the nucleus if the edge gradient on any side is quite small. Also there are a lot of variations outside the cell region thus sometimes making it harder for GVF to converge to the cell boundary. Further improvements can be made in GVF segmentation by smoothing the cell image using anisotropic diffusion thus making cell variations lesser. For cell classification, we have found that although 15 out of 18 features are significant, still the classification accuracy is not quite good (80.71%).A possible solution to this is to incorporate other features also like distances between cells and cell nucleus to cytoplasm ratio. Also we can employ backpropagation based neural network to improve over the classification accuracy.

Bibliography

[1] Jadhav., A.S, Banerjee, S., Dutta, P.K., Paul, R.R., Pal, M., Banerjee P., Chaudhuri, K, Chatterjee ,J., 2006. Quantitative analysis of histopathological features of precancerous lesion and condition using image processing technique. 19th IEEE Int. Symposium on Computer-Based Medical Systems. 231-236.

[2] Mukherjee ,A ., Paul, R. R., Chaudhuri, K., Chatterjee, J., Pal, M ., Banerjee, P.. 2006. Performance analysis of different wavelet feature vectors in quantification of oral precancerous condition, Oral Oncology.42, 914 - 928.

[3] Muthu Rama Krishnan,M., Pal,M., Bomminayuni,S,K., Chakraborty,C., Paul,R,R., Chatterjee,J., Ray,A,K., 2009. Automated classification of cells in sub-epithelial connective tissue of oral sub-mucous fibrosis-An SVM based approach. Computers in Biology and Medicine, 39, 12, 1096- 1104.

[4] Prabhu, S,R., Wilson, D,F., Daftary, D,K., Jhonson, N,W., 1992. Oral diseases in the Tropics: Oxford University Press.

[5] Chang,R,F., Chen,C,J., and Ho,M,F.,2004. Breast Ultrasound Image Classification Using Fractal Analysis. Proceedings of the Fourth IEEE Symposium on Bioinformatics and Bioengineering (BIBE'04).

[6] Tilakaratne, W., Klinikowski, M., Saku, T., Peters, T., Warnakulasuriya, S., 1997 Oral submucous fibrosis: Review on aetiology and pathogenesis. Oral Oncology. 42, 561-568.

[10] Duncan J. S., and Ayache, N., 2000. Medical image analysis: Progress over two decades and the challenges ahead. IEEE Transactions on Pattern Analysis and Machine Intelligence. 22, 85-106.

[11] Lessmann, B., Nattkemper, T, W., Hans, V, H., and Degenhard, A., A method for linking computed image features to histological semantics in neuropathology. Journal of Biomedical Informatics. 40, 631-641.

[12] Qian, W., Zhukov, T., Song, D,S., and Tockman, M, S.,2007. Computerized analysis of cellular features and biomarkers for cytologic diagnosis of early lung cancer. Analytical and Quantitative Cytology and Histology.29,103-111.

[13] Sertel, O., Kong, J., Shimada, H., Catalyurek, U., Saltz, J, H., and Gurcan, M., 2008. Computer-aided prognosis of neuroblastoma: Classification of stromal development on whole-slide images - art. no. 69150P.Medical Imaging 2008: Computer-Aided Diagnosis, Pts 1 and 2. 6915, P9150- P9150.

[14] Ferrari, R,J., Rangayyan, R,M., Desautels, J,E,L., Frere, A,F., 2001. Analysis of asymmetry in mammograms via directional filtering with Gabor wavelets, IEEE Transactions on Medical Imaging. 20,9, 953 - 964 .

[15] Wu,C,M., Chen,Y,C., Hsieh,K,S., 1992. Texture features for classification of ultrasonic liver images, 11, 2, 141 - 152.

[16] Marghani, K, A., Dlay, S, S., Sharif, B, S., and Sims, A., 2003. Morphological and texture features for cancers tissues microscopic images. Medical Imaging and Image Processing. 5032, 1757- 1764.

[17] Alexandratou, E., Yova, D., Gorpas, D., Maragos, P., Agrogiannis, G., and Kavantzas, N., 2008.Texture analysis of tissues in Gleason grading of prostate cancer - art. no. 685904. Imaging, Manipulation, and Analysis of Biomolecules, Cells, and Tissues Vi. 6859, D. L. Farkas, D. V. Nicolau, and R. C. Leif, Eds.85904-85904.

[18] Wiltgen, M., Gerger, A., Wagner, C., Bergthaler, P., and Smolle, J., 2007. Evaluation of texture features in spatial and frequency domain for automatic discrimination of histologic tissue. Analytical and Quantitative Cytology and Histology. 29, 251-263.

[19] Gonzalez, R, C, Woods, R, E., 2002. Digital Image Processing, 2nd Edition. Prentice Hall

[20] J.G. Daugman:"Uncertainty relations for resolution in space, spatial frequency, and orientation optimized by two-dimensional visual cortical filters", Journal of the Optical Society of America A, 1985,vol. 2, pp. 1160-1169.

[21] A. K. Jain, F. Farrokhnia, "Unsupervised texture segmentation using Gabor filters,"*Pattern Recognition*, vol. 24, no. 12, pp.1167-1186, 1991

[22]Manjunath, B, S., Ma, W,Y., 1996."Texture features for browsing and retrieval of image data". IEEE Transaction in Pattern Analysis and Machine Intelligence, 18, 837–842.

[23]Ojala, T., Pietikainen, M., Maenpaa, T., 2002. "Multiresolution gray-scale and rotation invariant texture classification with local binary patterns", IEEE Transactions on Pattern Analysis and Machine Intelligence, 24, 7, 971 – 987.

[24] Cheng-Lung Huang, Hung-Chang Liao, Mu-Chen Chen . "Prediction model building and feature selection with support vector machines in breast cancer diagnosis"

[25] Vapnik, 1995. Vladimir N. Vapnik, The nature of statistical learning theory, Springer-Verlag New York, Inc., New York, NY, 1995

[26] DiZenzo, S., 1986. A note on the gradient of a multi-image. Computer Vision Graphics Image Process. **33**, pp. 116–125

[27] Cumani, A., 1991. Edge detection in multispectral images. Comput. Vision Graphics Image Process.: Graphical Models Image Process. 53, pp. 40–51

[28] Haris, K., Efstratiadis, S., Maglaveras, N. and Katsaggelos, A., 1998. Hybrid image segmentation using watersheds and fast region merging. IEEE Trans. Image Process. 7 12, pp. 1684–1699

[29] Sijbers, J., Scheunders, P., Verhoye, M., Linden, A.V.D., Dyck, D.V. and Raman, E., 1997. Watershed segmentation of 3D MR data for volume quantization. Magnetic Resonance Imaging 15 6, pp. 679–688

[30] Vincent, L., 1993. Morphological grayscale reconstruction in image analysis: Applications and efficient algorithms. IEEE Trans. Image Process.2 2, pp. 176–201

[31]L Vincent, P Soille ,1991.Watersheds in digital spaces: an efficient algorithm based on immersion simulations.IEEE Transactions on Pattern Analysis and Machine Intelligence Volume: 13, Issue: 6, Publisher: IEEE Computer Society, Pages: 583-598

[32]Huang,P.W.[Po-Whei],Lai,Y.H.[Yan-Hao].Effective segmentation and classification for HCC biopsy images,Elsevier, PR(43), No. 4, April 2010, pp. 1550-1563.

[33] C. Xu and J.L. Prince, ``Gradient Vector Flow: A New External Force for Snakes,'' Proc. IEEE Conf. on Comp. Vis. Patt. Recog. (CVPR), Los Alamitos: Comp. Soc. Press, pp. 66-71, June 1997

[34]Robert M. Haralick,"Statistical and structural approaches to texture",*Proc. IEEE*, vol. 67, no. 5, pp. 786-804, 1979.